Characterization of a microflow cytometer with an integrated three-dimensional optofluidic lens system

M. Rosenauer and M. J. Vellekoop
Institute of Sensor and Actuator Systems, Vienna University of Technology, Gusshausstrasse 27-29/E366, 1040 Vienna, Austria

(Received 28 July 2010; accepted 25 September 2010; published online 30 December 2010)

Flow cytometry is a standard analytical method in cell biology and clinical diagnostics and is widely distributed for the experimental investigation of microparticle characteristics. In this work, the design, realization, and measurement results of a novel planar optofluidic flow cytometric device with an integrated three-dimensional (3D) adjustable optofluidic lens system for forward-scattering/extinction-based biochemical analysis fabricated by silicon micromachining are presented. To our knowledge, this is the first planar cytometric system with the ability to focus light three-dimensionally on cells/particles by the application of fluidic lenses. The single layer microfluidic platform enables versatile 3D hydrodynamic sample focusing to an arbitrary position in the channel and incorporates integrated fiber grooves for the insertion of glass fibers. To confirm the fluid dynamics and raytracing simulations and to characterize the sensor, different cell lines and sets of microparticles were investigated by detecting the extinction (axial light loss) signal, demonstrating the high sensitivity and sample discrimination capability of this analysis system. The unique features of this planar microdevice enable new biotechnological analysis techniques due to the highly increased sensitivity. © *2010 American Institute of Physics.* [doi:10.1063/1.3502672]

I. INTRODUCTION

In recent years, the determination of analytical relevant characteristics of single cells, viruses, or molecules plays an essential role in the interdisciplinary field of microfluidics and biotechnological research. Flow cytometry is often applied as a solution to difficult bioanalytical problems and provides an excellent method for fast quantification of different sets of analytes.[1] In many cases, cell populations are pretreated with markers or vital dyes to enable diagnostic screening of cell activities and functions such as cell cycle steps, viability, or biochemical cell kinetics.[2] A still quite common but manual method for cell viability screening is the trypan blue cell exclusion and methylene blue staining method. The combination of a light microscope and a hemocytometer is used to investigate viable cell populations including concentration and ratio for maintaining optimum culture conditions in bioreactors.[3] Although, most of the large flow cytometric benchtop systems equipped with multiple laser lines and several detection heads are able to perform automated and highly sensitive ananlytical measurement steps, including forward/side scatter and multicolor fluorescence detection, the costs of acquisition of these complex instruments are high. Throughout the last two decades, integrated silicon micromachining techniques have enabled new flow cytometric platforms smaller in size and less expensive to achieve the abovementioned goals with different methods (e.g., fluorescence illumination,[4–6] extinction,[7,8] and scattering measurements[9–11]). Besides these main motivation factors, novel measurement and sample handling methods were successfully introduced and have been further developed to competitive diagnostic products.[12] Nevertheless, in search for the simple and effective killer application,[13] novel optical techniques for increased sensitivity and reliable single cell analysis utilizing setups without single photon counting units can be an attractive solution for enhanced low-cost/low-power cell parameter screening. For successful single cell analysis, three major steps need to be implemented

in an integrated flow cytometer. First, the sample cell/bead suspension needs to be hydrodynamically sheathed and focused by a surrounding buffer fluid to the center of the microchannel to ensure a stable cell line-up. In microfluidics, the usually occurring laminar flow regime is often utilized for particle focusing and fluid sheathing purposes.[14–21] Second, after hydrodynamic centering, the sample should pass an optical inspection region where the single particles are illuminated individually by a focused incident light beam. For detecting the interaction of the incident light and single cells/particles, which is the third major step, conventionally fluorescence and extinction/scattering signals need to be strongly amplified, e.g., by single photon counting units. Since the light irradiance I $[W/m^2]$ coupled in the microfluidic channel codetermines the sensitivity of the micro total analysis system, polymer and fluidic lenses for in-plane light collimation/focusing are applied to increase the detection sensitivity and allow a more precise quantification. Two-dimensional microlenses have been presented in a multitude of publications, showing the tremendous interest to enhance and enable new measurement techniques. Besides fixed focal length lenses[9,22,23] fabricated by standard soft lithography, techniques to produce adjustable lenses are introduced. Generating versatile modifiable on-chip lenses by reshaping the surface curvature brings additional functionality to the microsystem. Recent publications have shown a novel method combining optics and microfluidics—optofluidics—to form micro-optical elements by manipulation of a core (body) and a cladding fluid. By carefully choosing these fluids, a well-defined interface between the refractive indices due to the laminar flow regime in the channel is given. This can be utilized for waveguides,[24–26] couplers,[26] and, most important for this study, lenses.[27–32] Even though most of these designs present excellent two-dimensional focusing abilities, displaying their great potential for many applications, a limit is reached when a focused spot in three dimensions is needed.

Recently, we presented the design, rapid fabrication, and proof-of-principle measurements of an optofluidic microdevice with the ability to focus an incident light beam three-dimensionally.[30] By altering the flow rate ratio, we were able to adjust the lens curvatures in the horizontal and vertical planes. The implementation of a hydrodynamic tunable lens with the ability to focus the illumination light in the center of the analytical channel increased the light irradiance significantly. The optofluidic microstructure and a stable beam spot size allows an accurate detection of light signal variations due to passing beads/cells, which is crucial for the functionality and quality of the device. A recently presented three-dimensional (3D) hydrodynamic focusing technique[23] in combination with an optofluidic adjustable 3D lens in the excitation light path fabricated in simple single layer fabrication applying inexpensive standard excitation/detection elements presents great potential for biotechnological experiments.

In this paper, we present the characterization results of an optofluidic lens system incorporated into a microflow cytometer with 3D hydrodynamic focusing performance along with a brief description of the fabrication methods. The coaxial (horizontal/vertical) sample alignment is achieved by reconfigurable three-dimensional hydrodynamic focusing in a single planar layer. Not only is it possible to achieve a well-focused centered sample stream, but the analyte can also easily be steered independently to an arbitrary position in the channel, which provides excellent flexibility for laboratory proof-of-concept tests and experiments. The bioassay sensitivity is significantly increased by the integration of a tunable optofluidic lens in combination with a planar biconcave air/resist lens in the incident optical path detached from the analysis channel geometry. To our knowledge, this is the first microflow cytometer system incorporating optofluidic elements that enable 3D focusing of the incident light beam used for the measurement of axial light loss due to passing cells/particles. The detection setup comprises a standard solid state laser and silicon photodiodes operated by lock-in-amplification as an alternative to single photon counting units. This research illustrates the applicability of compact low-cost/low-power elements for single cell analysis. After the technological aspects, a bioassay evaluation of the optofluidic-enhanced microflow cytometer measuring axial light loss signals of different sets of hydrodynamically focused *Saccharomyces cerevisiae* cells and polystyrene particles is presented. We investigated different sets of yeast cells in terms of viability and staining procedures by obtaining differences in peak height with an excellent reproducibility. The fabrication and packaging of the microflow devices

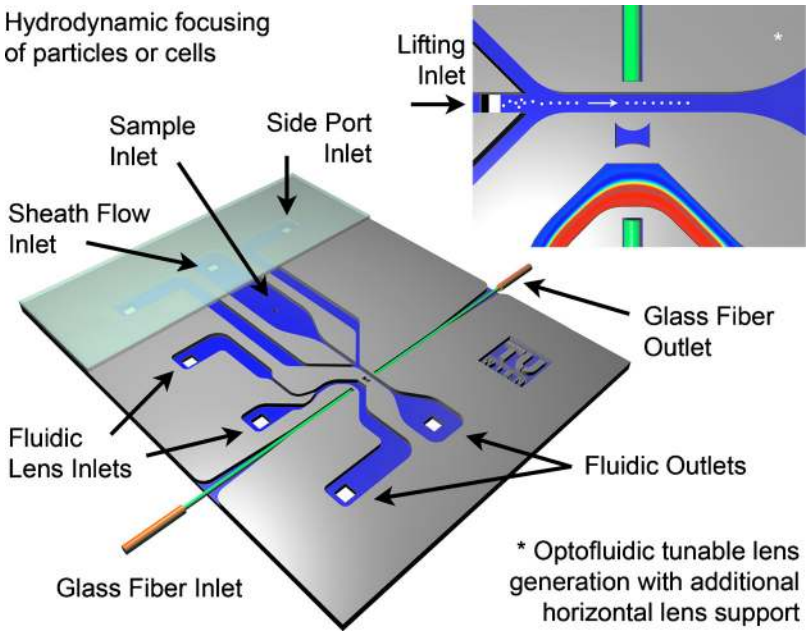

FIG. 1. Schematic of the flow cytometric device with an integrated optofluidic lens system to focus the incident light three-dimensionally on cells or particles.

are simple and fast, allowing a whole device wafer to be fabricated and characterized in less than one day.

II. EXPERIMENTAL

A. Materials

For the fabrication of the device, single-side polished 4-in. silicon wafers (thickness $=360$ μm) were purchased. The negative photoresist SU-8 2000 was supplied by Microchem (Newton, MA, USA) and the polydimethylsiloxane (PDMS) by Dow-Corning (Corning, NY, USA). For wafer processing and cleansing, standard chemicals, e.g., alkali hydroxide etchant-KOH, propylene glycol monomethyl ether acetate-PGMEA, ethanol, isopropyl alcohol, and acetone, were used (Sigma-Aldrich, St. Louis, MO, USA). In comparison to biological cell assays, commercially available cytometric standard particles provide an excellent measurement reference. Three different sizes of polystyrene beads (Fluka particles, var. coeff.$=1.5\%$, solid content 2%, Sigma-Aldrich, St. Louis, MO, USA) were used in the experiments: 4 (± 0.1) μm, 8 (± 0.2) μm, and 12 (± 0.2) μm, respectively. *S. cerevisiae* cells were kindly provided by the Analytical Biotechnology Group, Delft University of Technology (Delft, The Netherlands). For the cell cultivation, Dulbecco's Modified Eagle Medium was purchased from Invitrogen (Carlsbad, CA, USA) and Phosphate buffered saline (PBS) from Sigma Aldrich. Methylene Blue for cell staining and a Rhodamine B ethanol solution for light path visualization were supplied by Carl Roth (Karlsruhe, Germany).

B. Microfluidic design and fabrication

The optofluidic cytometer comprises three main components for a fully integrated, bioanalytical single cell assay: a single layer 3D hydrodynamic focusing design, integrated optical elements (fluidic and polymer lenses and fiber grooves) not influencing the microfluidic conditions, and axial light loss signal detection obtained by standard silicon photodiodes (Fig. 1). The design of the sensor system incorporates five hydrodynamic focusing inlets, two fluidic lens inlets, and two separate outlets. Since all fluidic inlets are placed on the bottom of the microchannel, the device

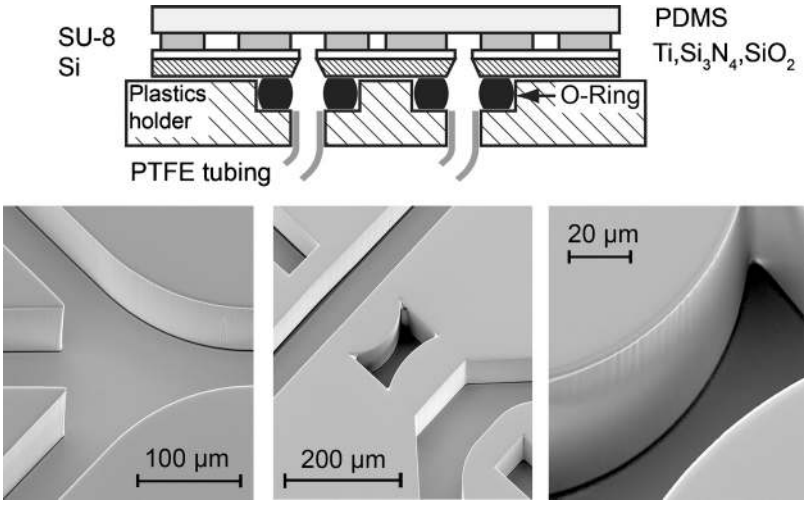

FIG. 2. Schematic cross-section of the fabricated microdevice mounted on a custom made plastics holder. Detailed SEM images of the inspection region and the air/resist lens chamber are shown.

fabrication was a straight-forward photolithographic process.[33] The optofluidic elements (channels, lenses, and fiber grooves) were fabricated in the negative photosensitive epoxy resist SU-8 on a standard 4-in. silicon wafer in a two mask process. First, the fluidic inlet holes were anisotropically backside etched by a 40% w/w KOH solution at 75 °C. The square inlet holes of the fluidic lens inlets, the two sideports, and the backside sheath flow as well as the outlets had a front side edge length of 250 μm. For the sample inlet and lifting ports, the silicon was etched to achieve an edge length of 80 μm. The silicon nitride layer on the front side of the wafer worked as an automatic etch stop. The second lithographic step applying a double-side mask aligner was used to structure the transparent, negative-working photoresist SU-8 on top of the silicon substrate. After soft-bake, cleaning, and hard-bake steps, a homogenous distribution with a film thickness of 82 μm was achieved. The channel width at the sample fluid entrance was 400 μm and narrowed down to 80 μm. The 45° adjacent sideport channels were also 80 μm broad. To ensure a homogeneous lifting of the sample, the total channel width was covered by the lifting inlet. The optofluidic lens channels were joined together to have a width of 80 μm and featured a 90° bend at the incident light path plane. The fiber grooves were 80 μm wide to allow the insertion of reduced-cladding multimode glass fibers. The air/resist lens featured a thickness of 80 μm and two different curvature radii ($r_1=150$ μm and $r_2=90$ μm). A PDMS cover lid (15×15 mm^2 and thickness=0.5 mm) bonded to a Pyrex glass slide was used as a waterproof gasket sheet on top of the microfluidic chip. The total area of the resulting microfluidic device was 9×13 mm^2. Figure 2 illustrates the results of the fabrication process of the sideport junction and the optical inspection region comprising the integrated optical lens. The surface roughness of the sidewalls is defined by the lithography process. The vacuum contact lithography step prevents mask projection faults, and the SU-8 structuring procedure[33,34] minimizes surface defects. An average sidewall surface roughness of $R_A=46$ nm was determined. By following the described simple single-layer procedure, a total fabrication time of less than 20 min for a single device was achieved. To secure the setup against mechanical vibrations and facilitate easy-to-handle chip packaging and cleaning, a plastics chip holder system mounted on a rearranged manual probe system including a light microscope was realized.

C. Detection system and data acquisition

The constituent parts of a similar setup have been described in detail elsewhere.[23] Briefly, the free-space solid state laser light ($\lambda=532$ nm, $P_{cw}=20$ mW, and $f_{max}=30$ kHz) was coupled in a glass fiber with reduced cladding (core/cladding=50/70 μm±2 μm, NA=0.22, Polymicro

Technologies, AZ, USA). The cleaved multimode fiber pigtails were inserted in the tapered fiber grooves at the incident side and at the outgoing side of the chip. The axial light loss due to particle absorption and refraction was measured by a standard silicon photodiode (350–1100 nm, 0.65 A/W at $\lambda = 970$ nm, 70 dB, Thorlabs, NJ, USA). The setup (laser and detectors) was operated in lock-in-amplification (Perkin Elmer 7265 Dual-Phase 250 kHz, Signal Recovery, Wokingham, United Kingdom) at 30 kHz. The current limitation of sample throughput is mainly defined by the applied maximal laser pulse frequency f_{max}, which results in practice in approximately 600 beads/s. An increase in throughput could be achieved by the application of a laser light source with a higher maximum pulse frequency. The signal of the photodiode was recorded and supplied as lock-in-amplifier input. After signal recovery, the output of the lock-in-amplifier was obtained by using the trigger events of the oscilloscope TDS2014 (Tektronix, OR, USA). The data acquisition and analysis software was written in MATLAB (The Mathworks, MA, USA).

D. Assay protocol

For the applied pressure-driven flow five syringe pumps (Chemyx Fusion 200, Chemyx, TX, USA) are used for sample, sheath, sideports, lifting, and fluidic lens flow rate supply. The two sideport flow rates are adjusted with a dual syringe pump to achieve a stable and even flow rate symmetry. To avoid *a priori* the introduction of air bubbles, the chip and the o-rings were first cleansed with ethanol. After aligning the microdevice on the holder, the microchannels are filled with the sheath medium and then sealed. For single cell/particle measurements, it is crucial that the densities of the buffer and sheath medium match the density of the particles to minimize particle sedimentation effects in the tubing and syringes (Note that in the microfluidic device, a particle/fluid density mismatch, e.g., de-ionized (DI)-water/polystyrene, does not affect the measurement data). Since polystyrene particles ($\rho = 1.05$ g/ml and $\eta = 1.5$ mPa s) are applied to proof the performance of the design an aqueous buffer solution of 14% (w/w) Sucrose (Sigma S9378–500 g) in 0.2 μm filtered de-ionized water was used. *Saccharomyces cerevisiae*, better known as baker's yeast, is commonly used for baking and brewing. It is one of the most studied eukaryotic model organisms in molecular and cell biology. Yeast cells have a diameter of 5–10 μm and are round to ovoid shaped. Culturing of yeast is achieved in two phases. First, yeast is streaked onto an agar plate, a sterile dish containing solidified growth medium, and left to grow at 28 °C overnight until enough yeast colonies are present. Subsequently, one colony is taken from the agar plate and put into a flask containing minimal medium, a growth medium only containing the bare essential nutrients. The flask is put into a shaking incubator at 28 °C until the desired cell density is reached.

III. RESULTS AND DISCUSSION

In this study, a microflow cytometer with liquid body–liquid cladding (L2) optical elements[35] enabling the simple reversible adjustments of optical parameters, e.g., lens curvature, waveguide dimension, and refractive index, by altering flow rates of the fluidic streams in the microsystem is investigated. Until now, 3D light focusing with solid elements has only been achieved with great fabricational effort by photolithographic structured multilayer devices. The following results of the introduced particle analysis system with the ability of hydrodynamic 3D light focusing illustrate the great potential in terms of accuracy, light focusing, and sample discrimination capability based on a simple fabrication method.

A. Coaxial hydrodynamic sample focusing

For reliable flow cytometry measurements, a stable and accurate sample alignment is necessary. To achieve this condition in microfluidics on an easy-to-fabricate microdevice, we realized a single-layer focusing method, which allows the adjustment of the cross-sectional area and position of the sample stream. The fluidic condition of the pressure-driven flow system was numerically simulated using COMSOL MULTIPHYSICS (Comsol Inc., Palo Alto, USA). Since the complete Navier–Stokes equations were used to derive the problem the inlet flows were defined as fully

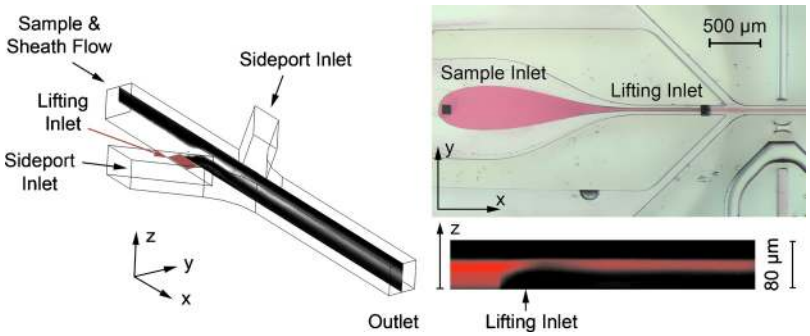

FIG. 3. Simulation results and light/confocal microscopy images of the hydrodynamic focusing of the microflow cytometer. (Left) CFD simulations (COMSOL MULTIPHYSICS) of the 3D sample sheathing. A centered cross-sectional XZ-plane illustrates the sample stream position (white) enfolded in the sheath medium (black). (Right) A micrograph (top) illustrates the focusing of red ink sample solution. The color intensity of the red ink solution decreases after the lifting inlet due to the reduced height of the lifted sample stream, which is completely surrounded by the transparent sheath flow (DI-water) after the lifting. A cross-sectional close-up of the lifting inlet and the following sideport junction illustrates the good agreement of theory and experiment of the sample centering.

developed (entrance length=1 m), and a no-slip condition at the channel walls was assumed. The diffusion coefficient[36] for fluorescent molecules was defined as $D=0.3–0.5\times10^{-9}$ m^2/s.

Figure 3 (left) shows the results of the numerical simulations. After introducing the sample to the microchip, it is overflown by the backside sheath flow and confined to the bottom of the channel. Through the tapering of the channel, the sample stream width is reduced, and by streaming over the lifting port, the analyte is shifted vertically. By applying a certain flow rate ratio, an optimum is reached where the sample centered.[19] Due to the parabolic flow velocity profile in the channel, the lifting procedure increases the sample width slightly, and therefore sideports are installed to define the final width. With the applied flow rates $Q_{sample}=1$ $\mu l/min$, $Q_{sheath}=50$ $\mu l/min$, $Q_{sideports}=5$ $\mu l/min$, and $Q_{lift}=20$ $\mu l/min$, a consistent cross-sectional spot of 12×14 μm^2 (width×height) is achieved both in computational fluid dynamics simulation and experiments. In Fig. 3 (right), the horizontal hydrodynamic focusing is illustrated with an aqueous red ink sample solution and de-ionized water as sheath fluid. To visualize the vertical centering, a Rhodamine B–ethanol solution was prepared. By confocal laser scanning microscopy (Nikon Eclipse C1 Plus, Nikon, Japan) the cross-section (XZ) of the microchannel was measured and is in good agreement with the simulations. Because of the flow velocities used, the influence of the diffusion is negligible. The Péclet number, Pe, describing the convection/diffusion dispersion, is in the range of 60 000, indicating that convection dominates the transfer.

B. Characterization of the 3D optofluidic light focusing

In this flow cytometric device, the advantages of 3D sample alignment and 3D light focusing are combined. The geometric design of the microchannels and the use of lens fluids with different refractive indices form an adjustable convex fluidic lens. Recently, we presented a fully adjustable three-dimensional lens with the possibility to reconfigure the lens curvatures independently.[30] Although this particular fluidic lens provides high functionality as tunable optical element, for the integration in a microflow cytometer the design, it is not optimal as only a centered focal spot is needed. To ensure uninfluenced biocompatible measurements, the analysis channel system is not connected to the optofluidic lens formation channels where two optical fluids ($n_{lens\ body}>n_{cladding}$) are introduced to the chip (Fig. 4). The fluid interface is arched to a convex form due to the geometry of the channel and the centrifugal force at the 90° bend.[30] To achieve overlapping focal lengths in the vertical and horizontal planes, an additional cylindrical air/resist lens with a thickness=80 μm, a first curvature radius $r_1=150$ μm, and a second curvature radius $r_2=150$ μm is integrated. The fluid conditions (optical channel geometry and velocity distribution) and the resulting focusing effect are determined by computational fluid dynamics (CFD) and

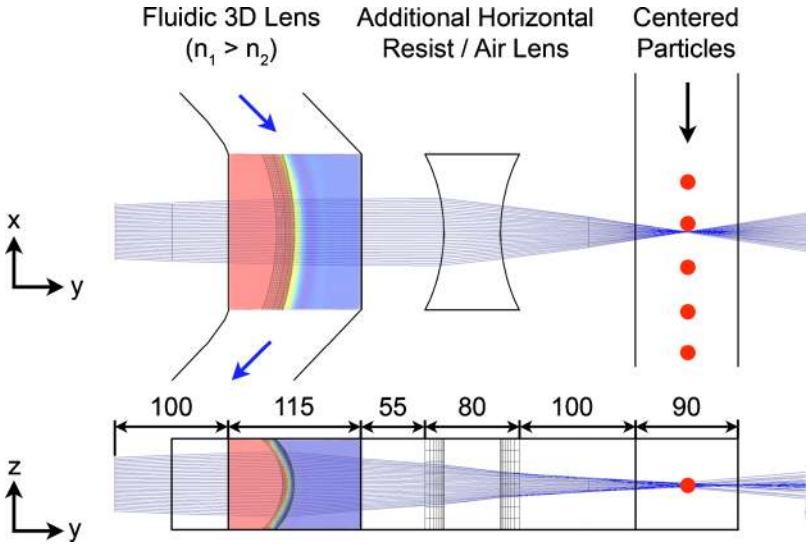

FIG. 4. Illustration of simulation results of the inspection region/fluidic lens system (COMSOL, ZEMAX). The interfaces of the transparent fluids with different refractive indices in both planes enable 3D light focusing. The polymer/air lens is integrated to achieve overlapping focal length in the horizontal and vertical planes.

raytracing simulations. In the simulation, fully developed flows with inlet rates $Q_{\text{lens body}} = 15\ \mu\text{l/min}$ and $Q_{\text{Cladding}} = 15\ \mu\text{l/min}$ are applied ($\text{Re} \sim 10$). The isosurface at half concentration ($c = 0.5\ \text{mol/m}^3$) between lens body ($c_0 = 1\ \text{mol/m}^3$) and cladding ($c_0 = 0\ \text{mol/m}^3$) inlet concentrations in the fluidic simulation is used as lens surface for the raytracing simulations. To evaluate these results and measure the extinction and forward scattering of specific analytes, glass fibers with a numerical aperture NA = 0.22 are inserted.

To characterize the 3D lens shaping, two optical transparent fluids are introduced to the microchip—lens body fluid 1: benzothiazole C_7H_5NS ($n_D^{22} = 1.64$ and $\rho = 1.246\ \text{g/cm}^3$); cladding fluid 2: mixture of 59% trichloro-trifluoroethan $C_2Cl_3F_3$ ($n_D^{22} = 1.36$ and $\rho = 1.563\ \text{g/cm}^3$); and 41% ethanol ($n_D^{22} = 1.36$ and $\rho = 0.79\ \text{g/cm}^3$). To visualize the optical focusing effect, a fluorescence micrograph was taken with an ethanol Rhodamine B solution filled analytical channel (Fig. 5).

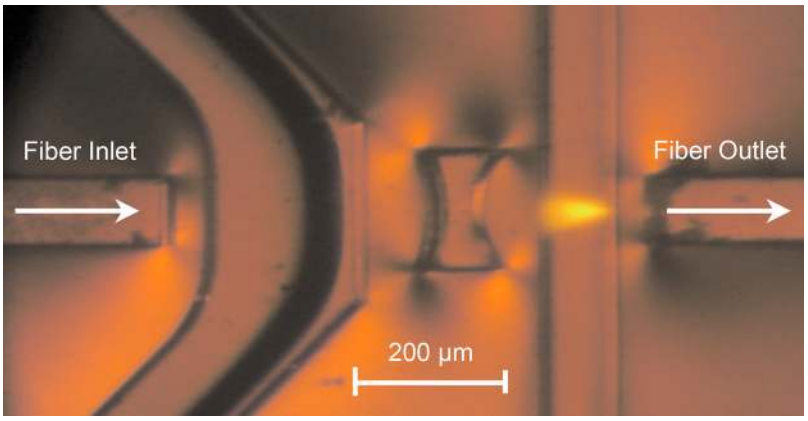

FIG. 5. Fluorescence micrograph of the optical inspection region. The analysis channel is filled with a Rhodamine B Ethanol solution to visualize light focusing. Glass fibers are inserted for illumination and detection purposes. The optical transparent fluids (lens body and cladding) are driven through the fluidic lens channel.

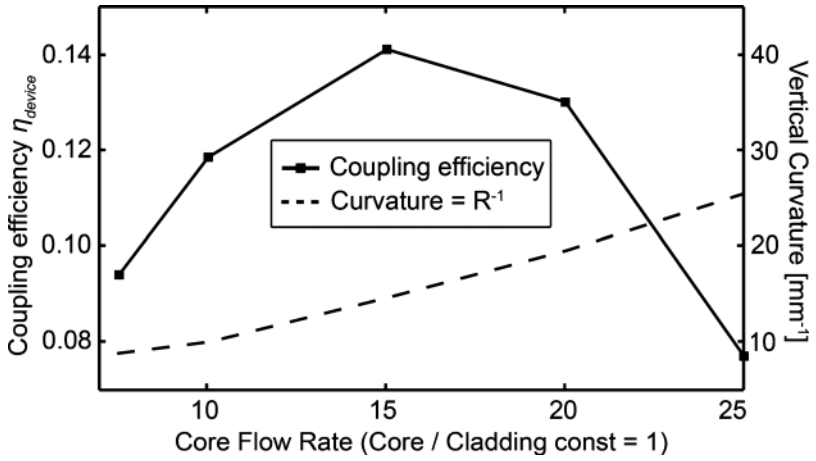

FIG. 6. Measured coupling efficiency and vertical curvature as a function of the absolute lens flow rates to quantitatively evaluate the focusing capability. The losses are measured by filling the analytical channel with an aqueous Ethanol solution (50% w/w). The connecting lines are for visualization only. Without the optofluidic lens, the maximum channel coupling efficiency is $\eta_{device}=0.06$ (benzothiazole-filled lens channel).

For a more extensive characterization of the fluidic lens, we experimentally determined the coupling efficiency η through the microfluidic device as a function of the absolute fluidic lens flow rates with a constant lens body/cladding flow rate ratio (Fig. 6). The coupling efficiency[37] is defined as

$$\eta_{total} = P_{out}/P_{source} = \eta_{source,fiber}\,\eta_{device}\,\eta_{fiber,detector},$$

with the measured optical power P_{out}, the laser source power $P_{source}=20$ mW and the fixed coupling factors $\eta_{source,fiber}$, $\eta_{fiber,detector}$, and the variable η_{device}. The output power was measured with a handheld laser power meter (Ophir Nova II) at $\lambda=532$ nm and an averaging time of 5 s. We determined the fixed coupling factors for free-space laser to fiber connection via an aspheric fiber coupler $\eta_{source,fiber}=0.69$ and from the fiber via the aspheric fiber coupler to the detector $\eta_{fiber,detector}=0.69$. The variable coupling efficiency η_{device} is influenced by the axial light loss (scattering, refraction) through the fluidic lens, the fixed air/polymer lens, and the analytical microfluidic channel. First, we investigated the coupling performance with an air-filled analytical channel. Due to the significant difference in refractive index between SU-8 and air, scattering at the channel walls take place, decreasing the coupling efficiency to a minimum of $\eta_{device}=0.04$. More important for the application was the scenario where the channel was filled with an aqueous ethanol solution (50% w/w), increasing the overall coupling efficiency (Fig. 6). By altering the absolute fluid lens flow rates, we were able to shift the position of the focal spot in the analytical channel. With increasing the absolute flow rates, the microlens curvature increases, thus intensifying the light focused into the detection fiber. After reaching a maximum in coupling efficiency through the chip, $\eta_{device}=0.14$ and a total efficiency $\eta_{total}=0.067$ at $Q_{lens\ body}=Q_{cladding}=15\ \mu l/min$, the measured signal power decreases. This phenomenon occurs because a further increase in total flow rate focuses the light before it reaches the fiber aperture (overfocused), causing the decrease in coupling efficiency. A similar method as proof-of-principle measurement is shown in the literature.[27,30] The vertical lens curvature is in almost linear relationship to the absolute flow rate values. In a quantitative comparison with microdevices without the optofluidic lens structures[23] comparable to state-of-the-art planar designs, an increase in coupling efficiency through the integrated lens and an improvement in signal-to-noise ratio for particle measurements by 4 dB were measured.

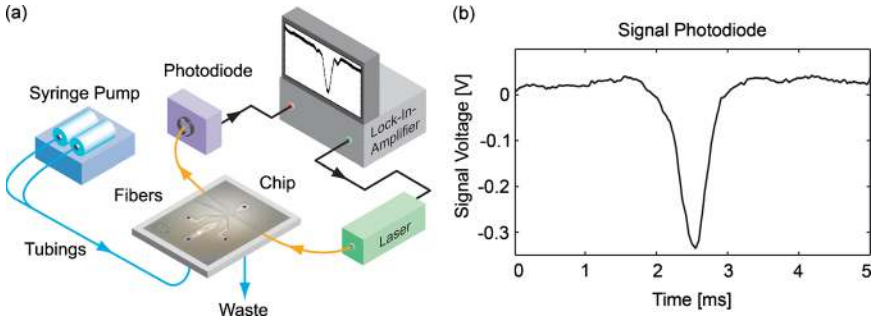

FIG. 7. (a) Optofluidic measurement setup with standard silicon laser/photodiode and lock-in-amplification. The fluid supply is obtained with infuse/withdraw syringe pumps. (b) Measurement signal of a single event (axial light loss) of a polystyrene particle ($d=12$ μm) passing the inspection region without the fluidic lens effect. The peak voltage drop is $V=-0.33$ V, and the duration is approximately 1 ms depending on the signal fluctuation at the entrance and exit of the particle in the light beam.

C. Setup evaluation with polystyrene microparticles

In this section, the performance of the measurement setup applying an inexpensive standard laser source and a standard silicon photodiode (30 dB preamplified) operated in lock-in-amplification ($f=30$ kHz) is evaluated [Fig. 7(a)]. The extinction or axial light loss signal is measured to characterize the intrinsic structural particle parameters like size and shape. In the next section (Sec. III D), a cell viability assay based on this technique is presented to discriminate between stained and unstained yeast cells.

First, the microbeads ($d=12$ μm) are suspended in density-matched buffer [polystyrene particles $\rho=1.05$ g/cm^3, buffer medium 14% (w/w) aqueous sucrose solution] and pressure-driven through the tubing and introduced to the microchip. The presimulated flow rates were supplied by syringe pumps (sheath/sample/lifting/sideport=5/0.1/2/0.5 μl/min). Consequently, a single centered polystyrene bead passes the inspection region interacting with the incident light beam focused on the center region of the channel. A detectable amount of light is blocked and/or scattered, allowing the phase-sensitive circuit to extract the variation and display it on the oscilloscope in ac-mode. In Fig. 7(b), a single event of a 12 μm polystyrene bead is illustrating the excellent detection performance of the microflow cytometer. To evaluate the performance of the device in terms of flow stability and detection accuracy, we investigated statistical parameters of the bead suspension by analyzing 1000 extinction events. A mean value $\mu=-0.335$ V, a standard deviation $\sigma=0.026$ V and a coefficient of variation CV=7.8% was obtained. In comparison with other fabricated microcytometer,[8,9,23] the results illustrate that the system provides high accuracy and reliability when a stable fluidic lens condition is obtained.

Furthermore, we investigated iteratively the different lensing phases to determine the output difference (Fig. 8). A particle suspension ($d=8$ μm) is prepared and hydrodynamically centered in the channel. In the process of characterizing, the liquid lens secured the setup against mechanical vibrations. The stability of the lens shape can be influenced by the syringes (glass/plastic), the pumping motion (stepper motor), and the fluidic interconnection setup (shock damped). Mechanical distortions are minimized by mounting the setup on a customized manual probe head placed on an optical table (Note that for reliable measurements, it is necessary that the lens fluid conditions are stable and variations in flow rates are eliminated). For preparation, the lens channels are flushed with an ethanol-DI-water solution to eliminate air bubble generation and adhesion in the fluidic lens region. The procedure is started by introducing the lens body fluid in the optofluidic channel. The absolute lens flow rates are Q=15 μl/min as determined in Sec. III B. The particles are hydrodynamically centered and interact with the incident light. The average peak height of the axial light loss voltage drops is $V=-0.07$ V. Only the cylindrical air/polymer lens focuses the excitation light. In the next step, the syringe pump supplying the cladding fluid introduces the second lens fluid to the device. After stabilization of the fluidic condition in the channel, the

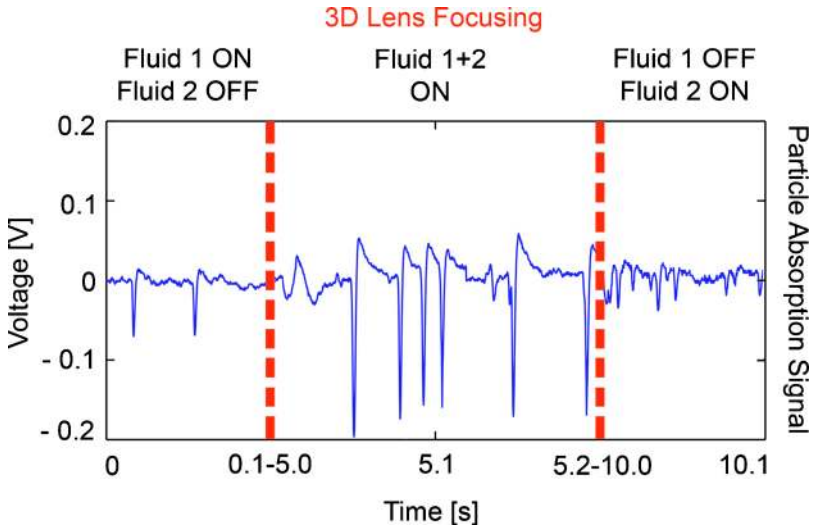

FIG. 8. Light intensity signal (extinction peaks) of the photodetector with polystyrene particles ($d=8$ μm) and fluidic lens adjustments. Fluid 1 is the lens body fluid with the high refractive index $n_1=1.64$. Fluid 2 is the cladding fluid with a refractive index $n_2=1.36$. The dashed lines can be understood as time steps of t=5 s until the fluidic lens condition reaches a stable shape.

convex fluidic lens is shaped in the vertical and horizontal plane. This is also illustrated by an increased height of the peak drop. The average peak height of the axial light loss voltage drops is $V=-0.18$ V. To complete the fluidic lens cycle in the final step, fluid 1—lens body fluid—is turned off, allowing the cladding fluid to completely fill the channel. A smaller peak height is obtained due to increased refraction at the channel walls. The measurement cycle and the highly increased peak height (3D lens focusing region) hereby excellently demonstrate the efficiency of our optofluidic enhancement.

D. Biological detection assays

In the final part, we investigate the applicability of the system as microbiological assay. The methylene blue staining procedure is applied to determine the viability of a yeast suspension. Based on the assumption that methylene blue enters a yeast cell, the enzymes of a healthy cell are breaking down methylene blue leaving the cell colorless. A dying or dead cell does not produce these enzymes, which results in coloration of the cell. To confirm the results, we measured the same treated sample with a hemocytometer manually.

As methylene blue rapidly becomes toxic, it is essential that the measurements (microflow cytometer and hemocytometer) are conducted within 15 min of preparation. After the cultivation of the yeast cells (see Sec. II D), the culture is suspended in PBS buffer for the staining procedure. A 0.1% methylene blue PBS solution is prepared and filtered to eliminate aggregates or clusters. The PBS cell suspension and the methylene blue solution are mixed equally (1:1).

The sample suspension is introduced and hydrodynamically centered in the microfluidic device. To minimize light scatter and refraction at the interfaces of sample and sheathing fluids, the buffer medium also consists of the same PBS-methylene blue solution. The fluidic lens is operated at Q=15 μl/min, and the lock-in-amplification for the extinction measurements is operated at a frequency $f=30$ kHz. The threshold value for recording events was set to $V_{\text{threshold}}=0.02$ V. After extinction peak data collection of around 900 trigger events per single test run, a data processing program based on MATLAB was realized to automatically determine the peak height of every single event for a statistical analysis. In Fig. 9, the results illustrate the excellent discrimination capability simply by measuring the light absorption, which is significantly increased by methylene blue staining. If we define a threshold value in peak height at $V=0.2$ V to determine the viability of the suspension, we obtained 705 nonstained cells from a total of 898 reliable cell counts (uncertain

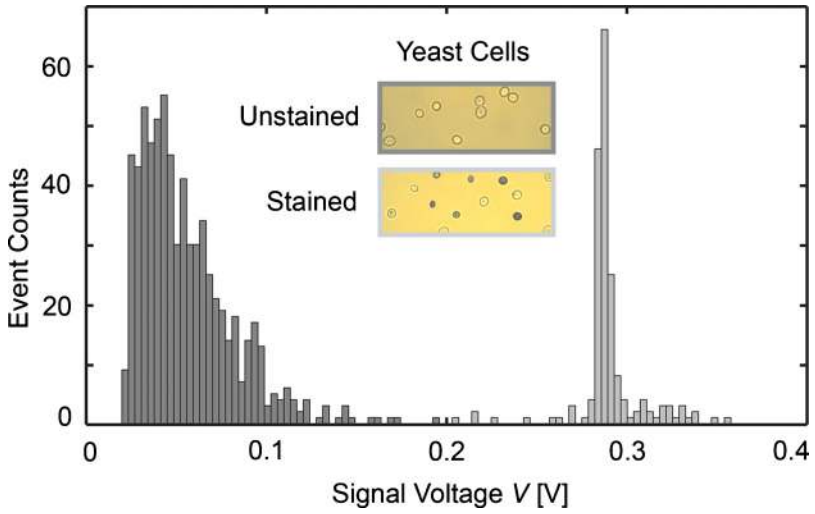

FIG. 9. Statistical evaluation histogram of the axial light loss measurement data. Counts/signal-voltage measurement of methylene blue stained yeast cells. Due to the increased light absorption when a stained cell passes through the inspection spot, the peak drop is higher than with unstained yeast cells. Therefore, it is possible to evaluate the viability in a fast and reliable way.

counts were reviewed and if necessary eliminated). A viability of 0.79 was determined applying this automated microdevice method. Simultaneously, the same yeast suspension was inspected with a hemocytometer and yielded a viability of 0.77. These results display a very good agreement of both microflow cytometer and standard reference measurements. Work is in progress to further investigate novel design ideas to integrate additional functional elements enabling simultaneous cytometer operations such as forward/side scattering and fluorescence detection.

IV. CONCLUSION

The presented single layer system demonstrated distinct advantages in terms of 3D sample focusing combined with 3D light focusing over conventional planar devices and allowed more sensitive measurements for on-chip analysis. The incorporated fluidic lens system was characterized, and it demonstrated the increased detection sensitivity due to the achieved narrow focal spot. We succeeded in detecting polystyrene microparticles and minimizing coupling losses in the incident light path. The detection of particles (4 μm) without the use of single photon counting units was possible. In terms of throughput, this system is comparable with state-of-the-art proof-of-principle systems with a nominal rate of approximately 600 beads/s. The optofluidic microflow cytometer demonstrated the excellent capability for biological viability assays determining the statistic distributions of stained and unstained yeast cells by measuring the axial light loss due to extinction. The measurement setup incorporating off-chip standard devices such as laser-diodes, multimode fibers, and a Si-photodiode was designed to contain low-cost equipment to facilitate simple modifications for various types of assays and possible integration of those elements in future developments.

ACKNOWLEDGMENTS

For the fabrication and the technical support, we thank E. Svasek and P. Svasek (ISAS, ZMNS, Vienna University of Technology). For the biotechnological support, we thank the group of P. Verhaert (Analyltical Biotechnology Group, Delft University of Technology, The Netherlands). The SEM image analysis was carried out using facilities at the University Service Centre for Transmission Electron Microscopy (USTEM, Vienna University of Technology).

[1] H. Shapiro, *Practical Flow Cytometry*, 4th ed. (Wiley, New York, 2003).
[2] C. E. Sims and N. L. Allbritton, Lab Chip **7**, 423 (2007).
[3] A. B. Hanley, J. McBride, S. Oehlschlager, and E. Opara, Toxicol. In Vitro **13**, 847 (1999).
[4] Y. C. Tung, M. Zhang, C.-T. Lin, K. Kurabayashi, and S. J. Skerlos, Sens. Actuators B **98**, 356 (2004).
[5] X. Wu, C. H. Chon, Y.-N. Wang, Y. Kang, and D. Li, Lab Chip **8**, 1943 (2008).
[6] S. Chiavaroli, D. Newport, and B. Woulfe, Biomicrofluidics **4**, 024110 (2010).
[7] A. Kummrow, J. Theisen, M. Frankowski, A. Tuchscheerer, H. Yildirim, K. Brattke, M. Schmidt, and J. Neukammer, Lab Chip **9**, 972 (2009).
[8] L.-M. Fu, R.-J. Yang, C.-H. Lin, Y.-J. Pan, and G.-B. Lee, Anal. Chim. Acta **507**, 163 (2004).
[9] Z. Wang, J. El-Ali, M. Engelund, T. Gotsæd, I. R. Perch-Nielsen, K. B. Mogensen, D. Snakenborg, J. P. Kutter, and A. Wolff, Lab Chip **4**, 372 (2004).
[10] J. P. Golden, J. S. Kim, J. S. Erickson, L. R. Hilliard, P. B. Howell, G. P. Anderson, M. Nasir, and F. S. Ligler, Lab Chip **9**, 1942 (2009).
[11] H. T. Chen and Y.-N. Wang, Microfluid. Nanofluid. **6**, 529 (2009).
[12] A. Arora, G. Simone, G. B. Salieb-Beugelaar, J. T. Kim, and A. Manz, Anal. Chem. **82**, 4830 (2010).
[13] N. Blow, Nat. Methods **4**, 665 (2007).
[14] A. Wolff, I. R. Perch-Nielsen, U. D. Larsen, P. Friis, G. Goranovic, C. R. Poulsen, J. P. Kutter, and P. Telleman, Lab Chip **3**, 22 (2003).
[15] C. Simonnet and A. Groisman, Appl. Phys. Lett. **87**, 114104 (2005).
[16] R. Yang, D. L. Feeback, and W. Wang, Sens. Actuators, A **118**, 259 (2005).
[17] C. C. Chang, Z. X. Huang, and R. J. Yang, J. Micromech. Microeng. **17**, 1479 (2007).
[18] C. H. Tsai, H. H. Hou, and L. M. Fu, Microfluid. Nanofluid. **5**, 827 (2008).
[19] G. Hairer and M. J. Vellekoop, Microfluid. Nanofluid. **7**, 647 (2009).
[20] M. G. Lee, S. Choi, and J.-K. Park, Lab Chip **9**, 3155 (2009).
[21] X. Mao, S.-C. S. Lin, C. Dong, and , T. J. Huang, Lab Chip **9**, 1538 (2009).
[22] S. Camou, H. Fujita, and T. Fujii, Lab Chip **3**, 40 (2003).
[23] M. Rosenauer, W. Buchegger, I. Finoulst, P. Verhaert, and M. J. Vellekoop, "Miniaturized flow cytometer with 3D hydrodynamic particle focusing and integrated optical elements applying silicon photodiodes," Microfluidics Nanofluidics (to be published).
[24] X. C. Li, Appl. Phys. Lett. **93**, 193901 (2008).
[25] M. Rosenauer and M. J. Vellekoop, Appl. Phys. Lett. **95**, 163702 (2009).
[26] D. B. Wolfe, R. S. Conroy, P. Garstecki, B. T. Mayers, M. A. Fischbach, K. E. Paul, M. Prentiss, and G. M. Whitesides, Proc. Natl. Acad. Sci. U.S.A. **101**, 12434 (2004).
[27] X. Mao, J. R. Waldeisen, and T. J. Huang, Lab Chip **7**, 1260 (2007).
[28] S. K. Y. Tang, C. A. Stan, and G. M. Whitesides, Lab Chip **8**, 395 (2008).
[29] Y. C. Seow, A. Q. Liu, L. K. Chin, X. C. Li, H. J. Huang, T. H. Cheng, and X. Q. Zhou, Appl. Phys. Lett. **93**, 084101 (2008).
[30] M. Rosenauer and M. J. Vellekoop, Lab Chip **9**, 1040 (2009).
[31] C. Song, Lab Chip **9**, 1178 (2009).
[32] N.-T. Nguyen, Biomicrofluidics **4**, 031501 (2010).
[33] P. Svasek, E. Svasek, B. Lendl, and M. Vellekoop, Sens. Actuators, A **115**, 591 (2004).
[34] C. H. Lee, K. Jiang, and G. J. Davies, Mater. Charact. **58**, 603 (2007).
[35] G. M. Whitesides, Nature (London) **442**, 368 (2006).
[36] K. Pappaert, J. Biesemans, D. Clicq, S. Vankrunkelsven, and G. Desmet, Lab Chip **5**, 1104 (2005).
[37] H. S. Cho, W. H. Kim, and H.-H. Park, Opt. Lasers Eng. **42**, 503 (2004).